IEEE Access
Multidisciplinary | Rapid Review | Open Access Journal

Received February 19, 2019, accepted February 28, 2019, date of publication March 13, 2019, date of current version April 5, 2019.

Digital Object Identifier 10.1109/ACCESS.2019.2904745

Direct Vibration Force Suppression for Magnetically Suspended Motor Based on Synchronous Rotating Frame Transformation

CONG PENG, (Member, IEEE), AND QIAN ZHOU

College of Automation Engineering, Nanjing University of Aeronautics and Astronautics, Nanjing 211106, China
Key Laboratory of Navigation, Control and Health-Management Technologies of Advanced Aerocraft, Nanjing University of Aeronautics and Astronautics, Nanjing 211106, China
Ministry of Industry and Information Technology and Jiangsu Key Laboratory of Internet of Things and Control Technologies, Nanjing University of Aeronautics and Astronautics, Nanjing 211106, China

Corresponding author: Cong Peng (pengcong.2006@163.com)

This work was supported in part by the National Natural Science Foundation of China under Grant 61703203, in part by the Natural Science Foundation of Jiangsu Province under Grant BK20170812B, and in part by the Project funded by the Priority Academic Program Development of Jiangsu Higher Education Institutions.

ABSTRACT Vibration force is critical in the normal operation of magnetic bearings. Among all vibration forces, the synchronous vibration force rising from rotor mass unbalance is the most influential factor. To effectively suppress the unbalance force for the high-speed magnetically suspended rotor, in this paper, a novel method for active magnetic bearings based on the synchronous rotating frame (SRF) transformation is developed. First, the structure and principle of SRF transformations for the magnetic bearing system is improved. Subsequently, different from the zero current suppression, the magnetic bearing force is directly set as the input of the vibration suppression, which is zero force suppression. In order to maintain the system stability, stability analysis, which is related to the plug-in vibration suppression algorithm, is conducted. Only one parameter needs to adjust to ensure the stability of the whole closed-loop system. Compared with the conventional method of vibration force suppression, the proposed method has better performance. The simulation and experimental results on a magnetic suspended motor system demonstrate that the proposed SRF-based method can effectively suppress the synchronous vibration force.

INDEX TERMS Synchronous rotating frame (SRF) transformation, active magnetic bearing (AMB), vibration force, synchronous current.

I. INTRODUCTION

As is a non-contact support structure, magnetic bearings have many promising and practical advantages over conventional mechanical bearings such as compact structure, lower rotating frictional loss, lubrication elimination and higher rotational speed. According to the structure and control system of the magnetic bearings, it can be divided into two categories: active magnetic bearing and passive magnetic bearing. Active magnetic bearing (AMB) is drawing increasing interest due to its inherent characteristics like adjustable stiffness and flexible control in all DOFs [1]–[5]. Therefore, active magnetic bearings are widely used in both civil and military applications, like high speed motor, molecular pump and spacecraft attitude actuator [6]–[10].

Despite their advantages, vibration caused by unbalance mass of rotor and sensor runout is a serious challenge in rotating machinery. Vibration contains Synchronous vibration and multi-frequency vibration [11], [12]. Then mass unbalance coupled with the residual displacement caused by the supported position difference between the balancer and the AMBs lead to the generation of synchronous vibration force. Synchronous vibration caused by mass unbalance of rotors has the maximum amplitude and mainly affect the performance of AMBs. Mass unbalance of rotors, resulting from the principle of geometry axis is not coincident with its inertial axis [13]. Vibration force with small amplitude and high frequency can leads to serious damage effects [14]–[16]. Especially, when the rotor rotates at a very high speed, the

The associate editor coordinating the review of this manuscript and approving it for publication was Luigi Biagiotti.

vibration force turns more severe, as the centrifugal force which is proportional to the square of the rotational speed. For most of the AMB-based machines, synchronous vibration force transferred to the outside through the casing can generate noise, vibration and even can damage mechanical equipment. Although the mechanical balancing of rotors can reduce part of the vibration force, residual part of imbalance remains due to the change of working condition. Hence, it is necessary to adopt active control algorithm to suppress synchronous vibration force of AMBs as much as possible.

There are many previous researches on vibration suppression of AMB control system. The mainly two classes of control strategies for real time vibration suppression including auto balancing control and unbalance compensation control. For the former method, the synchronous component of control current is suppressed to force the rotor to rotate around the inertial axis, in this way the synchronous vibration force can be reduced, known as zero magnetic force control. For the latter method, synchronous component in displacement signal is concerned to force the rotor to rotate around the geometric axis, known as zero displacement control. A variety of approach such as notch filter [17]–[19], state observer based control strategy [20], learning based algorithm [21] were adopted to eliminate the synchronous vibration. Moreover, a least-mean-square (LMS) based algorithm was proposed to compensate the synchronous current by feeding forward compensation component to control current [22]. However, LMS based algorithm has fixed step, which is a hard tradeoff between stability and convergence speed of system. This method is only suitable for several specific speed. Another repetitive learning algorithm was proposed to adjust learning rate adaptively, which can suppress synchronous current in large speed range [23]. These two methods mentioned above can suppress the vibration force caused by the synchronous current but hardly can eliminate the residual one caused by the negative displacement stiffness. Liu *et al.* [24] adopted the negative displacement stiffness compensation in current loop. In this method, the inertia axis position identified in high rotational speed was used to eliminate the synchronous vibration force in relatively low rotational speed. Nevertheless, this approach did not consider the low-pass features of the amplifier. It would accumulate the phase error of the open-loop compensation over time, and further weaken the compensation effect. Moreover, although the power amplifier parameters can be obtained by offline testing [25], an offline amplifier model at the whole rotational speed range did not compensate the complete vibration force in time.

To achieve rapid compensation effect, Zheng *et al.* [26] proposed a synchronous rotating frame (SRF) based method, in which SRF-based transformation method was adopted to eliminate the synchronous current. but the method did not consider the residual synchronous component by negative displacement stiffness. The SRF-based method was applied in induction motors and power electronics for a long time [27], [28], but seldom applied in complete vibration force suppression of active magnetic bearing. Previous researches on vibration force suppression of AMBs cover diverse situations. The methods mentioned above lack of concerning the negative displacement stiffness of AMBs or complicated computation so they hardly can be adopted in real application.

In this study, an improved synchronous vibration force suppression algorithm based on SRF transformation is proposed. A compact and practical controller for vibration suppression is plugged into the baseline control system of magnetically suspended rotor. The basic idea of the proposed method is to set the unbalanced force as the direct input of the vibration suppression controller. SRF transformation can track the harmonic signal of a certain frequency and apply the real-time compensation. There are mainly three advantages of the proposed method. First, the synchronous vibration force is completely suppressed by direct force compensation. Second, the SRF based controller is compact in structure for easy implementation and can reduce the computation burden. Third, only one parameter needs to adjust to achieve the overall system stability.

The rest of paper is arranged as follows. In section II, a model of magnetic suspended rotor with mass unbalance is build. In section III, the proposed SRF-based synchronous vibration force method is analyzed and in section IV, simulation and experiment results are given. Conclusions are provided in Section V.

II. DYNAMIC MODELING WITH MASS UNBALANCE

The schematic diagram of magnetically suspended rotor with unbalanced mass is shown in Figure 1. The rotor is suspended by two radial magnetic bearings AMB1 and AMB2. In order to simplify the modeling analysis, three plans Π, Π_1, Π_2 are defined. The dynamics modeling is established on the assumption. 1) high speed magnetic suspended rotor is a rigid body, 2) magnetic field inhomogeneity of AMBs is neglected, 3) parameters of every radial channel are constant to each other.

According to Figure 1, there is obvious offset between the geometric axis from the inertial axis. The rotor mass eccentric lead to the misalignment of two axes. Due to the relationship between the geometric center and the mass center, we can

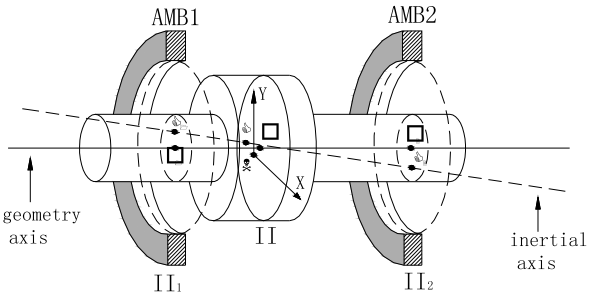

FIGURE 1. Basic Diagram of the AMB control system with unbalance rotor.

achieve:

$$\begin{bmatrix} X_A(t) \\ Y_A(t) \\ X_B(t) \\ Y_B(t) \end{bmatrix} = \begin{bmatrix} x_A(t) \\ y_A(t) \\ x_B(t) \\ y_B(t) \end{bmatrix} - \begin{bmatrix} \Theta_{Ax} \\ \Theta_{Ay} \\ \Theta_{Bx} \\ \Theta_{By} \end{bmatrix} \tag{1}$$

where X_A, X_B, Y_A, Y_B are displacement of geometric axis in plate Π_1 and Π_2, respectively and x_A, x_B, y_A, y_B are the displacement of inertial axis in plate Π_1 and Π_2, respectively.

Then we can set the disturbance as:

$$\begin{cases} \Theta_{Ax}(t) = l\cos(\Omega t + \varphi) - m\cos(\Omega t + \alpha) \\ \Theta_{Ay}(t) = l\sin(\Omega t + \varphi) + m\sin(\Omega t + \alpha) \\ \Theta_{Bx}(t) = l\cos(\Omega t + \varphi) + n\cos(\Omega t + \beta) \\ \Theta_{By}(t) = l\sin(\Omega t + \varphi) - n\sin(\Omega t + \beta) \end{cases} \tag{2}$$

where φ donates the initial phase of the unbalance force, Ω is the rotational speed of the magnetic suspended rotor. l, m, n are distance between OC, OC_1 and OC_2 respectively.

According to the dynamic characteristic of AMBs, the magnetic force equation is a nonlinear expression. When the rotor moves in a small area near the equilibrium position, by using the Taylor series expansion, the nonlinear equation of magnetic force can be linearized as:

$$\begin{cases} f_{Ax} = K_x X_A + K_{ix} i_{Ax}(X_A) \\ f_{Ay} = K_y Y_A + K_{iy} i_{Ay}(Y_A) \\ f_{Bx} = K_x X_B + K_{ix} i_{Bx}(X_B) \\ f_{By} = K_y Y_B + K_{iy} i_{By}(Y_B) \end{cases} \tag{3}$$

with

$$\begin{aligned} K_{ix} &= K_{iy} = 2N \cdot \frac{F_{pm} \cdot \mu_0 \cdot A}{\sigma \cdot \delta(2M_{pm} \cdot \mu_0 \cdot A + \delta)} \\ K_x &= K_y = -\frac{\mu_0 \cdot A \cdot F_{pm}^2}{\sigma^2 \cdot \delta} \cdot \left(\frac{1}{2M_{pm} \cdot \mu_0 \cdot A + \delta}\right) \end{aligned} \tag{4}$$

where f_{Ax}, f_{Ay}, f_{Bx} and f_{By} are the magnetic forces generated by bearings A and B in x and y directions, respectively. K_{ix}, K_{iy} and K_x, K_y donate the current stiffness and displacement stiffness of AMB, respectively.

Substituting (1) and (2) into (3), the equation of magnetic force can be written as:

$$\begin{cases} f_{Ax} = K_x(x_A(t) + \Theta_{Ax}) + K_{ix} i_{Ax}(x_A(t) + \Theta_{Ax}) \\ f_{Ay} = K_y(y_A(t) + \Theta_{Ay}) + K_{iy} i_{Ax}(y_A(t) + \Theta_{Ay}) \\ f_{Bx} = K_x(x_B(t) + \Theta_{Bx}) + K_{ix} i_{Bx}(x_B(t) + \Theta_{Bx}) \\ f_{By} = K_y(y_B(t) + \Theta_{By}) + K_{iy} i_{By}(y_B(t) + \Theta_{Bx}) \end{cases} \tag{5}$$

where Θ_{Ax}, Θ_{Ay}, Θ_{Bx}, Θ_{By} are displacement disturbance in A, B bearings generated by mass unbalance, respectively. According to (2), the Θ represents the disturbance caused by the mass unbalance of rotor. It can be derived that the frequency of unbalance disturbance is related to the fundamental frequency of rotor speed. Besides, it can be derived from (2) that the disturbance in direction A and B are quadrature, Θ_{Ax} is 90 degrees leading to Θ_{Ay} in phase. According to (5), both displacement component and current component of magnetic forces containing disturbances.

Hence, the generation of synchronous magnetic force not only results from synchronous control current fluctuation, but also induces by the residual synchronous component in negative displacement stiffness.

III. AN IMPROVED SRF BASED SYNCHRONOUS FORCE SUPPRESSION METHOD

A. THE PRINCIPLE OF SRF TRANSFORMATION

Previous research on frame transformation mainly focused on power electronic. AC vector can easily converted to DC vector in new frames for more accurate tracking. In order to extend the SRF transformation in the magnetically suspended rotor system, two coordinate systems based on the rotor mass center C and geometric center M is constructed. Figure 2 shows the schematic diagram of the coordinates transformation. Set C as the origin of the static reference frame CX_sY_s, M as the origin of the bearing-rotor coordinate CX_rY_r which rotates with the speed of Ω. It can be derived that the motion trajectory of the geometric center M is a circle with the mass center C. Therefore, the displacement coordinate of geometric center M in rotating frame is a constant vector.

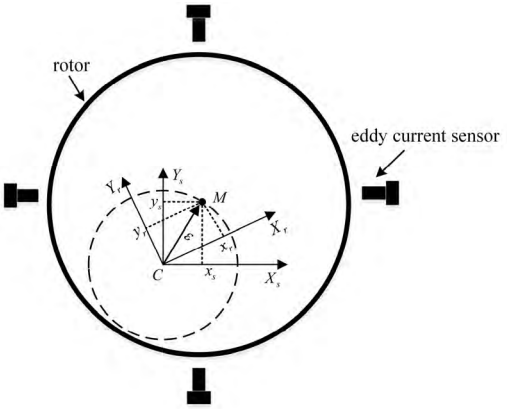

FIGURE 2. Schematic diagram of the basic rotating coordinate transformation.

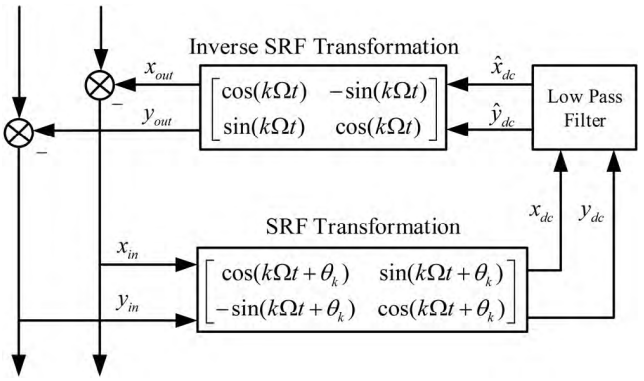

FIGURE 3. The structure of the control system with the synchronous rotating frame transformation.

The whole structure of the SRF transformation is shown in Figure 3. Let $[x_{in}, y_{in}]$ and $[x_{dc}, y_{dc}]$ represent the motion

coordinate of M in static reference frame and rotating frame, respectively. Then the relationship between the motion vector in two coordinates can be presented as,

$$\begin{bmatrix} x_{dc} \\ y_{dc} \end{bmatrix} = T(\Omega t) \begin{bmatrix} x_{in} \\ y_{in} \end{bmatrix} \tag{6}$$

with

$$T(\Omega t) = \begin{pmatrix} \cos(\Omega t + \theta_k) & \sin(\Omega t + \theta_k) \\ -\sin(\Omega t + \theta_k) & \cos(\Omega t + \theta_k) \end{pmatrix} \tag{7}$$

where $T(\Omega t)$ donates the SRF transformation. Ω is the rotational speed of the rotor. θ_k represents the compensation phase angle, which is further used to ensure the stability of the whole control system.

If the rotor rotates at a constant speed Ω, after the SRF transformation, the input signal is characterized with a dc component with mixed harmonic signal. The fundamental component can be extracted by a low-pass filter. Although higher-order filter can improve the filtering effect, it increases the calculation burden. Therefore, first-order filter is commonly employed as,

$$g_f(s) = \frac{k}{s + \tau} \tag{8}$$

Then, by applying an inverse SRF transformation and set the output of the first-order filter as the input of the inverse SRF transformation as follows, the synchronous vibration signal of the rotor can be deduced as,

$$\begin{pmatrix} x_{out} \\ y_{out} \end{pmatrix} = T_{inv}(\Omega t) \begin{pmatrix} \hat{x}_{dc} \\ \hat{y}_{dc} \end{pmatrix} \tag{9}$$

where $\hat{x}_{dc}$, $\hat{y}_{dc}$ are outputs of the first-order filters. x_{out}, y_{out} are the identified synchronous vibration signal, and $T_{inv}(\Omega t)$ is,

$$T_{inv}(\Omega t) = \begin{pmatrix} \cos(\Omega t) & -\sin(\Omega t) \\ \sin(\Omega t) & \cos(\Omega t) \end{pmatrix} \tag{10}$$

According to the location of the sensor, vibration signal in x and y axes have the same frequency but with phase difference of 90^o, so complex variable is adopted, yields,

$$X_{dc}(t) + jY_{dc}(t) = (X_{in}(t) + jY_{in}(t))e^{-j(\Omega t + \theta_k)} \tag{11}$$

The Laplace transform under zero initial condition is deduced as:

$$X_{dc}(s) + jY_{dc}(s) = (X_{in}(s - \Omega) + jY_{in}(s - \Omega))e^{-j\theta_k} \tag{12}$$

Typically, the transformation function of low-pass filter is,

$$G_f(s) = \frac{\varepsilon}{\lambda s + 1} \tag{13}$$

Then it can be obtained that

$$\begin{aligned} \hat{X}_{out}(s) + j\hat{Y}_{out}(s) &= (\hat{X}_{dc}(s) + j\hat{Y}_{dc}(s))e^{j\Omega t} \\ &= \hat{X}_{dc}(s - j\Omega) + j\hat{Y}_{dc}(s - j\Omega) \\ &= (X_{in}(s) + jY_{in}(s))\frac{\varepsilon}{(\lambda s - j\Omega) + 1}e^{-j\theta_k} \\ &= (X_{in}(s) + jY_{in}(s))G_k(s) \end{aligned} \tag{14}$$

where $G_k(s)$ is the open-loop transfer function of SRF. Hence, the SRF closed-loop transfer function can be derived as follows.

$$G_{fk}(s) = \frac{1}{1 + G_k(s)} = \frac{(\lambda s - j\Omega) + 1}{(\lambda s - j\Omega) + 1 + e^{-j\theta_k}\varepsilon} \tag{15}$$

The synchronous vibration force is directly set as the control target. The vibration force is constructed by synchronous current and displacement. Then set the synchronous vibration force as the input of the SRF.

Two main performance index of SRF transformation are notch depth and bandwidth. Compared to the conventional notch filter, the proposed SRF transformation contains an e item. This item can not only influences the whole frequency characteristics of the AMB system nearby the notch frequency Ω, but also let us configure the poles of the transfer function of the novel notch filter. The bode diagram of the SRF transformation is shown in Figure 4.

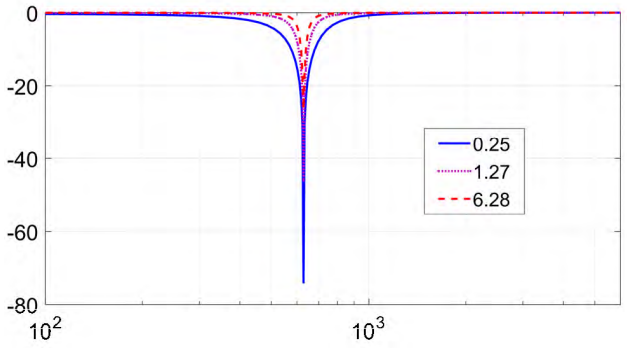

FIGURE 4. Bode diagram of SRF transformation with different coefficient γ.

The frequency characteristic of SRF transfer function is,

$$G_{fk}(j\omega) = \frac{1 + j(\lambda\omega - \Omega)}{1 + e^{-j\theta_k}\varepsilon + j(\lambda\omega - \Omega)} \tag{16}$$

By dividing a coefficient λ into (16), it can be written as,

$$G_{fk}(j\omega) = \frac{j\omega - j\Omega' + \gamma}{j\omega - j\Omega' + \gamma + e^{-j\theta_k}k} \tag{17}$$

In which, $\gamma = 1/\lambda$, $\Omega' = \Omega/\lambda$, $k = \varepsilon/\lambda$. Then, the amplitude-frequency character is,

$$\left|G_{fk}(j\omega)\right|_A = \sqrt{1 - \frac{2k\gamma e^{-j\theta_k} + k^2 e^{-2j\theta_k}}{\left(\gamma + ke^{-j\theta_k}\right)^2 + (\omega - \Omega')^2}} \tag{18}$$

It can be obviously seen from (18) that when $\omega \to \Omega'$ amplitude $\left|G_{fk}(j\omega)\right|_A \to 0$. Beside this the notch depth is related to the coefficient γ. It can be clearly seen from Figure 4 that with the increase of coefficient γ, the depth of bode diagram decreased.

B. IMPROVED SYNCHRONOUS FORCE SUPPRESSION WITH SRF-BASED METHOD

For reliability and robustness of the system, a proportional-integration- differentiation (PID) controller is adopted as the basic controller to trace the given current. The transfer function of controller $C(s)$, power amplifier $G_w(s)$ and rotor dynamics $P(s)$ are presented as follows

$$C(s) = k_p + \frac{k_I}{s} + k_D s \tag{19}$$

$$G_w(s) = \frac{k_w}{1 + \tau_w s} \tag{20}$$

$$P(s) = \frac{K_{ix}}{ms^2 - K_x} \tag{21}$$

where k_p, k_I, k_D represent the proportional, integration, differentiation coefficients, respectively. k_w and τ_w are the current gain and time constant value of the amplifier.

In this paper, the suppression of synchronous vibration force is mainly discussed. In order to eliminate the vibration force effectively, it is necessary to eliminate two parts forces, which are synchronous current stiffness force and synchronous component remaining in displacement stiffness. Generally, the current stiffness and displacement stiffness are known as constant values.

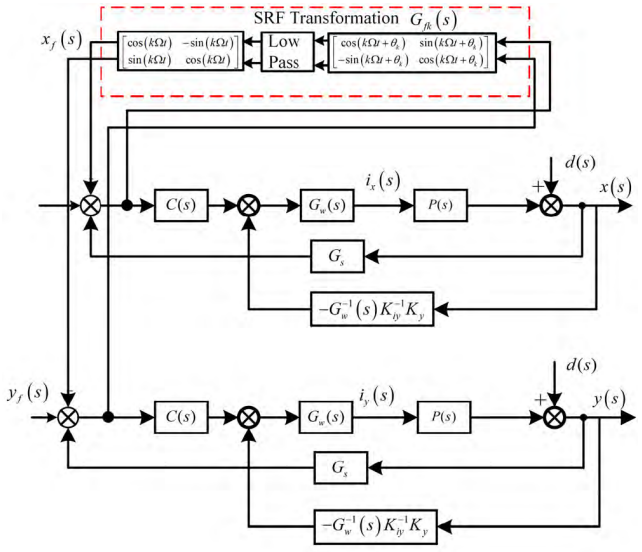

FIGURE 5. The control diagram for the complete synchronous vibration force suppression with the conventional scale compensation method.

Figure 5 presents the conventional SRF-based method for eliminating the synchronous vibration force. The basic principle is to identify the synchronous component of current. In this way, the SRF algorithm is introduced for the synchronous component identification. Then the current, which flows through the SRF, is feedback to the control loop to compensate the synchronous component. Hence, the input for the power amplifier is composed of two prats, one is generated by the baseline controller as $G_c(s)\left[x(s) - x_f(s)\right]$, the other is $-K_{ix}^{-1}K_x x(s)$, which comes from the component of the displacement stiffness. Then, the output current of the power amplifier is presented as,

$$i(s) = G_w(s)\left\{C(s)\left[x(s) - x_f(s)\right] - K_{ix}^{-1}K_x x(s)\right\} \tag{22}$$

Hence, the magnetically suspended force is calculated as,

$$\begin{aligned} F(s) &= K_x x(s) + K_{ix} i(s) \\ &= K_x\left[I - G_w(s)\right]x(s) + K_{ix}G_w(s)C(s)\left[(s) - x_f(s)\right] \end{aligned} \tag{23}$$

It can observed from (23), $\arg\left(G_w(j\omega)\right) \rightarrow 0$ and $G_w(j\omega) \rightarrow I$, when $\Omega \leq \omega_\omega(\omega_\omega$ is the cut-off frequency of the power amplifier). That is, the synchronous vibration force can be totally suppressed under a relatively low speed. However, when $\Omega >> \omega_\omega$, the low pass characteristic of the power amplifier is serious and the lag phase inevitably affects the compensation precision. There still remains synchronous component in the displacement stiffness. Consequently, the conventional scale compensation method has a significant negative impact on the suppression effect at high operational speed.

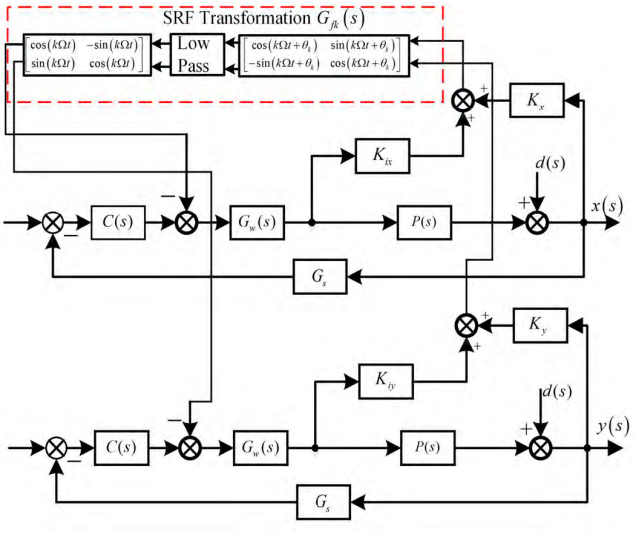

FIGURE 6. The control diagram for the complete synchronous vibration force suppression with the proposed direct force compensation method.

In order to improve the negative suppression impact at high speed, a direct magnetic force feedback control method which based on the SRF transformation is proposed and the block diagram is shown in Figure 6. According to Figure 6, The residual compensation for the displacement stiffness is proposed by feed the displacement signal into the SRF, in this way, displacement stiffness combined with current stiffness construct the direct magnetic force compensation. Hence, the direct magnetic force compensation component is designed as,

$$q(s) = G_{fk}(s)\left[K_{ix} i(s) + K_x x(s)\right] \tag{24}$$

Then the output current of the power amplifier can be written as,

$$\begin{aligned} i(s) &= [q(s) - C(s) K_s x(s)] G_w(s) \\ &= \left\{G_{fk}(s) [K_{ix} i(s) + K_x x(s)] - C(s) K_s x(s)\right\} G_w(s) \end{aligned} \tag{25}$$

Then,

$$i(s) = \frac{\left[G_{fk}(s) K_x - C(s) K_s\right] x(s) G_w(s)}{\left[1 - G_{fk}(s) G_w(s) K_{ix}\right]} \tag{26}$$

Hence, the magnetically suspended force is calculated as,

$$\begin{aligned} f(s) &= K_x x(s) + K_{ix} i(s) \\ &= K_x x(s) + K_{ix} \frac{\left[G_{fk}(s) K_x - C(s) K_s\right] x(s) G_w(s)}{\left[1 - G_{fk}(s) G_w(s) K_{ix}\right]} \end{aligned} \tag{27}$$

According to (27), the direct force compensation achieves the residual synchronous component in the displacement stiffness, and the low pass characteristic of the power amplifier is removed. It is superiority for the complete elimination of synchronous vibration forces. Furthermore, compared to the conventional scale compensation method, the direct force compensation method uses both current and displacement stiffness components to instead the displacement feedback component. It avoids the increase of the harmonic currents amplitude and dose not influence the system frequency characteristics over the low pass filter stopband. The residual compensation for the displacement stiffness is eliminated with the total force compensation.

C. STABILITY ANALYSIS

Based on the proposed control structure, the stability criterion is given by the layout of the roots of the characteristic equation. According to the overall system structure diagram, the characteristics polynomial of the closed-loop transfer function can be obtained as,

$$1 + K_{ix} G_c(s) G_w(s) P(s) - K_x P(s) + K_{ix} G_{fk}(s) G_w(s) = 0 \tag{28}$$

Substituting (15) into (28), then it can be written as:

$$\begin{aligned} &1 + K_{ix} G_c(s) G_w(s) P(s) - K_x P(s) + K_{ix} G_{fk}(s) G_w(s) \\ &= (\lambda s - j\Omega + \varepsilon + k e^{-j\theta_k}) + \frac{K_{ix}(\lambda s - j\Omega + \varepsilon) G_w(s)}{1 + K_{ix} G_c(s) G_w(s) P(s) - K_x P(s)} \end{aligned} \tag{29}$$

As described in [6], a sensitivity function is used to evaluate the stability. Set $S(s)$ as the sensitivity function of the control system, and it has the presentation as,

$$S(s) = \frac{K_{ix} G_w(s)}{1 + K_{ix} G_c(s) G_w(s) P(s) - K_x P(s)} \tag{30}$$

Assume that the system is stable before the SRF is plugged in. Then the ploys of $S(s)$ remain in left complex plane. Combining the sensitivity function with the characteristic polynomial, (30) can be simplified as,

$$(\lambda s - j\Omega + \varepsilon + k e^{-j\theta_k}) + (\lambda s - j\Omega + \varepsilon) S(s) = 0 \tag{31}$$

in which $k = \hat{k} K$, K is a constant value and $\hat{k}$ is a minimal value. Rewrite (31) as follows,

$$\begin{aligned} \varsigma(s, \hat{k}) &= (\lambda s - j\Omega + \varepsilon + \hat{k} K e^{-j\theta_k}) \\ &\quad + (\lambda s - j\Omega + \varepsilon) S(s) = 0 \end{aligned} \tag{32}$$

Only one ploy is obtained in characteristics polynomial, if $\hat{k} = 0$, where,

$$s = \frac{j\Omega - \varepsilon}{\lambda} \tag{33}$$

After the insertion of SRF method, the poles of the closed-loop system lie within a small region of $s = (j\Omega - \varepsilon)/\lambda$. According to (32), the derivative of s can be obtained when $\hat{k} = 0$ as follows,

$$\frac{\partial s(k)}{\partial k}|_{k=0} = -\frac{\partial \varsigma(s, \hat{k})}{\partial k} / \left(\frac{\partial \varsigma(s, \hat{k})}{\partial s}\right) = -\frac{K e^{-j\theta_k}}{\lambda(1 + S(j\Omega))} \tag{34}$$

In order to satisfy the stability requirements and ensure the motion of root locus to left after inserting the SRF, the real part of (34) needs to less than zero as follows,

$$\begin{cases} \mathrm{Re}\left[-\dfrac{K e^{-j\theta_k}}{\lambda(1 + S(j\Omega))}\right] < 0 \\ \mathrm{Im}\left[-\dfrac{K e^{-j\theta_k}}{\lambda(1 + S(j\Omega))}\right] = 0 \end{cases} \tag{35}$$

where $\mathrm{Re}[\cdot]$ denotes the real part and $\mathrm{Im}[\cdot]$ means imaginary part. The stability condition shows in (35) is equal to the equation as follows,

$$-\frac{\pi}{2} < \arg\left(\frac{K e^{-j\theta_k}}{\lambda(1 + S(j\Omega))}\right) < \frac{\pi}{2} \tag{36}$$

As can be concluded from (36) that, to satisfy the overall stability condition, the compensation angle θ_k needs to be adjusted with the change of rotor speed Ω. Therefore, based on the tuning process of the compensation angle, the stability and robustness of the overall system with the plug-in novel synchronous vibration suppression method can be guaranteed.

IV. SIMULATION AND EXPERIMENTAL RESULTS

A. EXPERIMENTAL SETUP

In order to validate the suppression performance of the novel SRF-based method for synchronous vibration force, a set of experimental system is set up in the laboratory. The control plant is an AMB supported permanent magnet synchronous motor which power is 11kW. The control board of AMB system containing dual-core processors. On one hand, the control algorithm mainly carried out by a high-speed Texas Instrument DSP (TMS320F28335). On the other hand, the inner current loop-tracking algorithm is implemented in an ALTERA FPGA (EP4CE10F17C8N). In this experimental system, for improving measurement accuracy, the rotor displacements are sampled by the eddy current sensors in difference form with a sample rate of 12.5 KHz. The switch

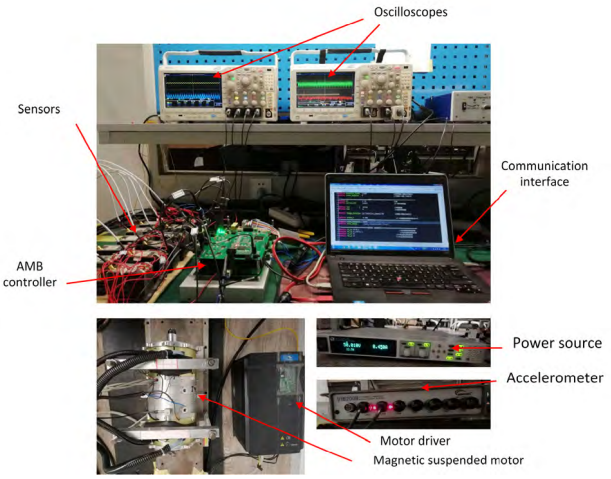

FIGURE 7. The experimental set-up.

amplifiers with H-bridge of the power MOSFET drive the magnetic bearings.

Figure 7 shows the experimental setup of the whole AMB control system. The vibration force is tested by a (VIB2008U) accelerometer. The vibration measure system is composed of a set of probes (ULT2401/V) and a signal processing unit. The vibration forces are measured by accelerate probes indirectly. According to the relationship between force and acceleration, the vibration force can be achieved. The acceleration data is recorded by the data grabber and further analyzed by the real-time multi-analyzer. The signal processing unit can analysis the force with both frequency and amplitude. Hence, the vibration force can be decomposed to different frequency components for further analysis.

B. SIMULATION RESULTS

In order to verify the effectiveness and feasibility of the direct vibration force suppression, control algorithm is carried out by an AMB model in Matlab/Simulink. Simulation parameters of AMB system are shown in Table 1. The system parameters implemented in simulation are obtained by real test and the same as those used in the experiment.

TABLE 1. Parameters of the AMB system.

Parameter	Value
Rotor mass *(m)*	15 kg
J_X , J_Y	0.062 kg · m^2
The polar moment of inertial (J_z)	0.102 kg · m^2
The displacement stiffness$(k_X$, $k_Y)$	9.5 × 10^5 N/m
The current stiffness$(k_{i\,x}$ ' $k_{i\,y})$	675 N/A
The proportional coefficient of PID(k_P)	0.28
The integral coefficient of PID (k_I)	4
The differential coefficient of PID(k_D)	0.0008

As mentioned previously, compensation angle θ_k plays a critical role for proposed method. To analysis the closed-loop system performance, the following six cases at the rotational speeds of 50 Hz, 100 Hz, and 200 Hz, with the compensation angle $\theta_k = 0, \pm\pi/2$ are carried out.

Case 1) The rotor speed is 50Hz with compensation angle $\theta_k = 0$.

Case 2 The rotor speed is 50Hz with compensation angle $\theta_k = \pi/2$.

Case 3) The rotor speed is 100Hz with compensation angle $\theta_k = 0$.

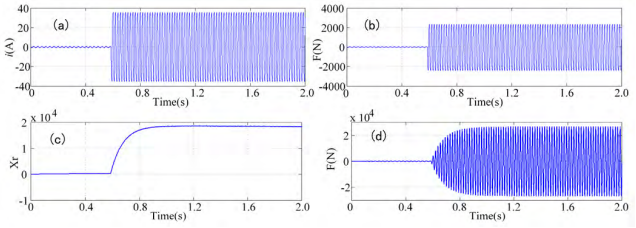

FIGURE 8. Simulation results of AMB control system using the proposed method in Case 1. The method is activated at $t = 0.5$s. (a) Control current. (b) Magnetic force. (c) Filter output. (d) Identified vibration force signal.

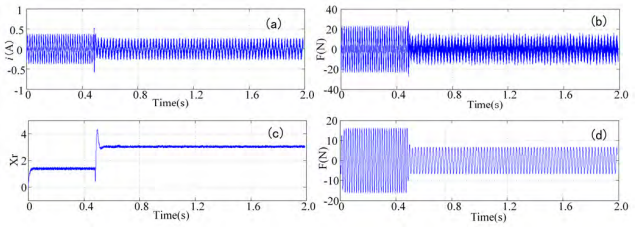

FIGURE 9. Simulation results of AMB control system using the proposed method in Case 2. The method is activated at $t = 0.5$s. (a) Control current. (b) Magnetic force. (c) Filter output. (d) Identified vibration force signal.

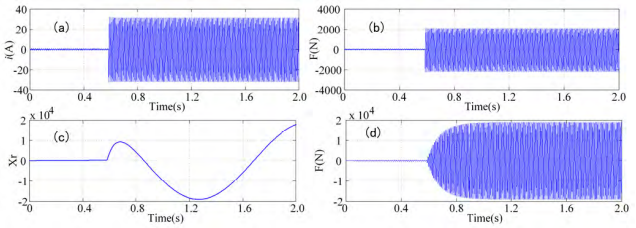

FIGURE 10. Simulation results of AMB control system using the proposed method in Case 3. The method is activated at $t = 0.5$s. (a) Control current. (b) Magnetic force. (c) Filter output. (d) Identified vibration force signal.

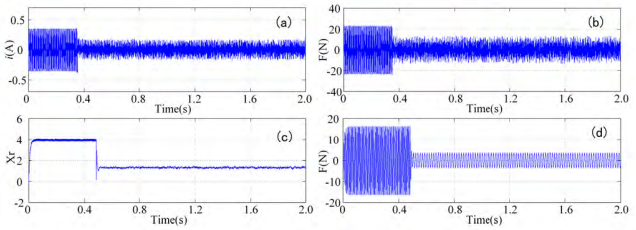

FIGURE 11. Simulation results of AMB control system using the proposed method in Case 4. The method is activated at $t = 0.5$s. (a) Control current. (b) Magnetic force. (c) Filter output. (d) Identified vibration force signal.

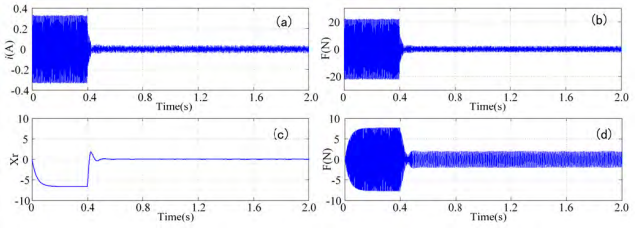

FIGURE 12. Simulation results of AMB control system using the proposed method in Case 5. The method is activated at $t = 0.5$s. (a) Control current. (b) Magnetic force. (c) Filter output. (d) Identified vibration force signal.

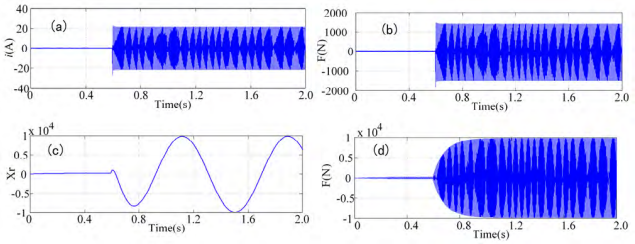

FIGURE 13. Simulation results of AMB control system using the proposed method in Case 6. The method is activated at $t = 0.5$s. (a) Control current. (b) Magnetic force. (c) Filter output. (d) Identified vibration force signal.

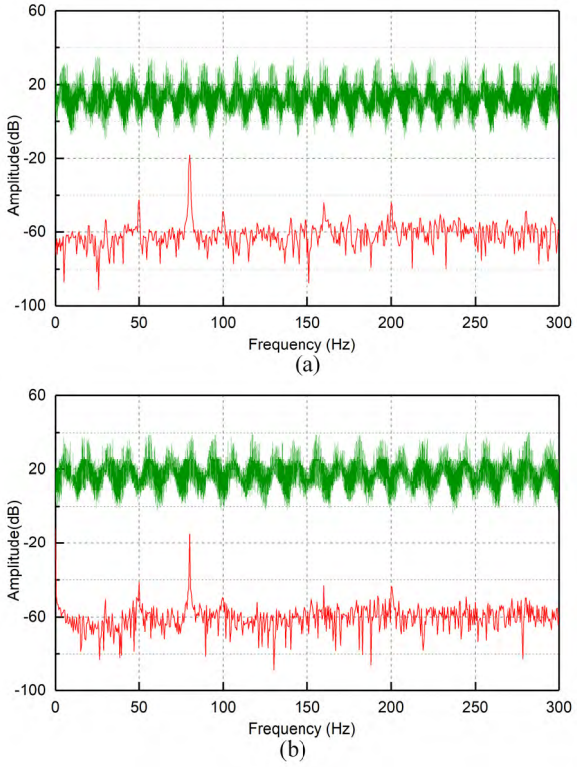

FIGURE 14. Experimental results for control current without any vibration suppression at the rotor speed of 80 Hz. (a) Results of channel X. (b) Results of channel Y.

Case 4) The rotor speed is 100Hz with compensation angle $\theta_k = -\pi/2$.

Case 5) The rotor speed is 200Hz with compensation angle $\theta_k = 0$.

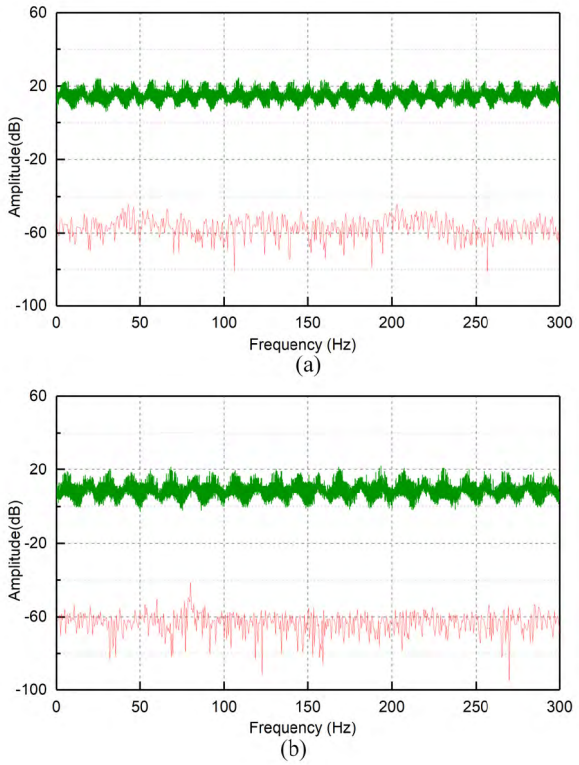

FIGURE 15. Experimental results for control current with the proposed vibration suppression at the rotor speed of 80 Hz. (a) Results of channel X. (b) Results of channel Y.

Case 6) The rotor speed is 200Hz with compensation angle $\theta_k = -\pi/2$.

Figures 8–13 illustrate the simulation results of the AMB system, when the rotor rotates at a speed of 50Hz(3000rpm), 100Hz (6000 rpm) and 200Hz(12000rpm), respectively. It can be obviously derived from Figure 8. and Figure 10. that when the rotational speed is relatively low, such as 50Hz, and with the compensation angle $\theta_k = 0$, the closed-loop control system is out of stable. As shown in Figure 9., by tuning the compensation angle θ_k to a proper value, the stability of the system is guaranteed. With the speed increasing, as is shown in Figure 11., the rotor speed is 100Hz and without compensation angle, the system is divergent. By adjusting compensation angle to $\theta_k = -\pi/2$, then the proposed vibration suppression method performs well.

When the rotational speed is high, the system becomes more stable. As shown in Figure 12, the speed of rotor is 200Hz and $\theta_k = 0$, the system is of convergence. On the contrary, with speed is 200Hz and $\theta_k \neq 0$, the system becomes unstable. The simulation results provide an evidence for system stability that the plugged-in suppression method for vibration force suppression has a negative effect on the stability of the closed-loop system, especially at low rotating speed. In [7] we can find the similar conclusion. That is, the divergence output of low-pass filter is the main cause for the system unstable.

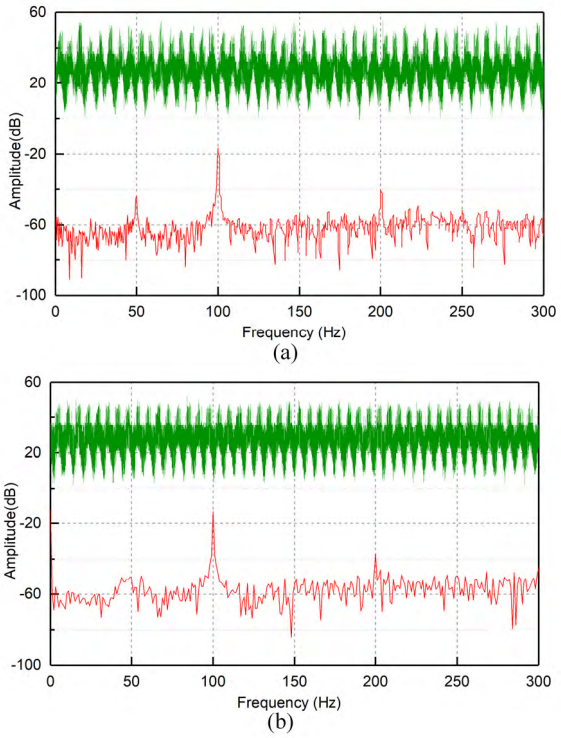

FIGURE 16. Experimental results for control current without any vibration suppression at the rotor speed of 100 Hz. (a) Results of channel X. (b) Results of channel Y.

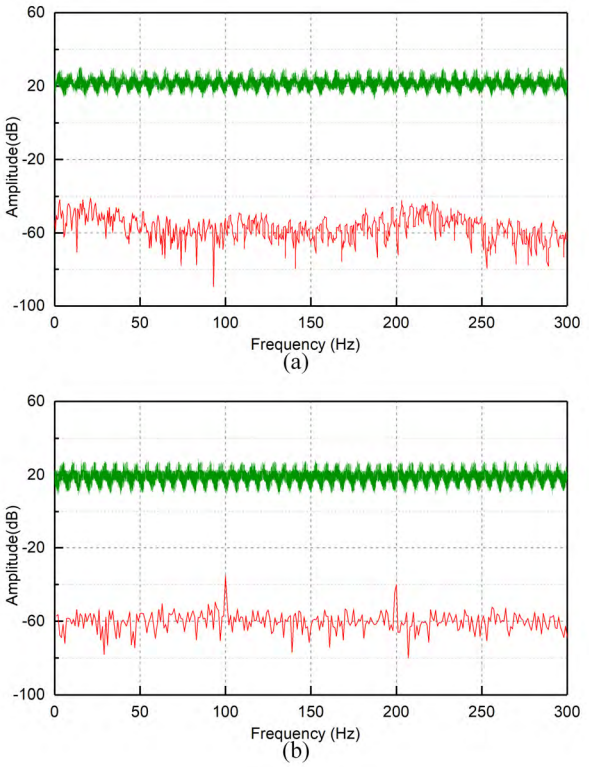

FIGURE 17. Experimental results for control current with the proposed vibration suppression at the rotor speed of 100 Hz. (a) Results of channel X. (b) Results of channel Y.

C. EXPERIMENTAL RESULTS

The experiment is carried out to validate the effect of proposed method. In practical application of the AMB motor, suitable compensation phases are concerned considering system stability and suppression performance. Figure 14 shows the experimental results at rotational frequency of 80Hz without using the proposed method. In Figure 14(a), for channel X, the amplitude of synchronous current is 0.38A and the corresponding fast Fourier transformation (FFT) result is shown below the control current. The peak value of the spectrum plot is −20dB. The vibration force is great tested by the accelerometer, it can transfer to the motor plate and cause damage. In Figure 14(b), for channel Y, the experimental result is similar to X. Figure 15 presents the experimental results of control current at the rotational frequency of 80Hz with the proposed SRF-based direct force suppression method. The compensation angle θ_k is set as 60^o to guarantee the closed-loop stability. Figure 15(a) and Figure 15(b) show the control current of channel X and Y respectively. It can be observed that the peak-peak value of synchronous current is 0.2A. The corresponding synchronous component are −48dB and −42dB, respectively. It is obviously that the synchronous component of control current is suppressed effectively with the magnitude drop of 81.7%. To validate the suppression effect in different rotation speed, another experiment was conducted at a rotational speed of 100Hz. From Figure 16(a) and Figure 16(b), it can be seen that the synchronous current component is large both in channel X and Y without any suppression algorithm plugged

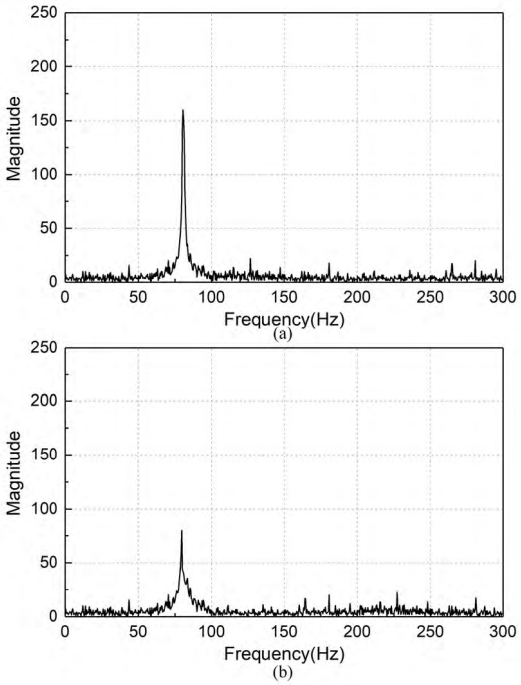

FIGURE 18. Experimental results of acceleration for vibration force testing at the speed of 80Hz. (a) Without any vibration suppression. (b) With the proposed method suppression.

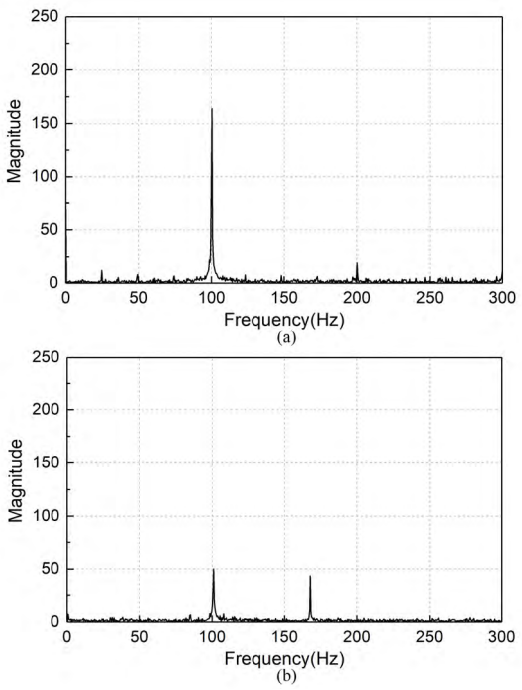

FIGURE 19. Experimental results of acceleration for vibration force testing at the speed of 100Hz. (a) Without any vibration suppression. (b) With the proposed method suppression.

in. To keep the system stable, the compensation angle was set as 45^o. According to the FFT analysis, the synchronous component is up to −19dB and −20dB, respectively. The other multi-frequency harmonics rise from the sensor runout and is not the main vibration components. After the proposed method added in, In Figure 17, the amplitude of the synchronous vibration is −50dB. By comparing Figure 16 with Figure 17, it can be concluded that the synchronous current suppression with proposed SRF-based control method is effective with the magnitude drop of 84.3%.

Furthermore, the vibration force signal in X and Y channel are captured by accelerometer. Experimental results are shown in Figure 18 and Figure 19. Figure 18(a) presents the result without eliminating synchronous current fluctuations and residual displacement component at a speed of 80Hz. Compared Figure 18(b) with Figure 18(a), vibration force is suppressed effectively with the magnitude drop of 85%. Figure 19 show the result conducted in a rotational speed of 100Hz. It can be seen that the synchronous vibration force is the dominant component among all harmonic vibrations. As is shown in Figure 19(b), by applying the proposed algorithm, the synchronous component of vibration is also effectively suppressed. This is consistent with the theoretical analysis.

V. CONCLUSION

In this paper, a novel SRF-based direct synchronous vibration force suppression method for the AMB motor control system is presented. Compared with the conventional method, this diagram concerns the presence of negative displacement stiffness. It can suppress the synchronous vibration force with high precision and great effective. In addition, the proposed SRF-based suppression method is easy to realize, so it can reduce the computation complexity of the controller and achieve a better performance. Moreover, the system stability can be guaranteed by tuning one parameter. The proposed method is compared with the conventional one. The comparative results demonstrate that the proposed SRF-based direct vibration force control method achieves superior performance.

REFERENCES

[1] J. Fang, S. Zheng, and B. Han, "AMB vibration control for structural resonance of double-gimbal control moment gyro with high-speed magnetically suspended rotor," *IEEE/ASME Trans. Mechatronics*, vol. 18, no. 1, pp. 32–43, Feb. 2013.

[2] C. Peng, J. Sun, X. Song, and J. Fang, "Frequency-varying current harmonics for active magnetic bearing via multiple resonant controllers," *IEEE Trans. Ind. Electron.*, vol. 64, no. 1, pp. 517–526, Jan. 2017.

[3] G. Schweitzer and E. H. Maslen, *Magnetic Bearings: Theory, Design, and Application to Rotating Machinery*. Berlin, Germany: Springer-Verlag, 2009.

[4] H. Gao, L. Xu, and Y. Zhu, "Compensation control of real-time unbalance force for active magnetic bearing system," *Trans. Nanjing Univ. Aero. Astro.*, vol. 28, no. 2, pp. 183–191, Jun. 2011.

[5] T. Baumgartner, R. M. Burkart, and J. W. Kolar, "Analysis and design of a 300-W 500 000-r/min slotless self-bearing permanent-magnet motor," *IEEE Trans. Ind. Electron.*, vol. 61, no. 8, pp. 4326–4336, Aug. 2014.

[6] J. Fausz, B. Wilson, C. Hall, D. Richie, and V. Lappas, "Survey of technology developments in flywheel attitude control and energy storage systems," *J. Guid. Control Dyn.*, vol. 32, no. 2, pp. 354–365, Mar./Apr. 2009.

[7] B. Han, Z. Huang, and Y. Le, "Design aspects of a large scale turbomolecular pump with active magnetic bearings," *Vacuum*, vol. 142, pp. 96–105, Aug. 2017.

[8] L. Ai *et al.*, "Research on a superconducting magnetic bearing system for submerged cryogenic disk motor-pump," *IEEE Trans. Appl. Supercond.*, vol. 28, no. 4, Jun. 2018, Art. no. 5202505.

[9] C. Di, L. Petrov, J. J. Pyrhönen, and X. Bao, "Unbalanced magnetic pull compensation with active magnetic bearings in a 2 MW high-speed induction machine by FEM," *IEEE Trans. Magn.*, vol. 54, no. 8, Aug. 2018, Art. no. 8202913.

[10] Q. Liu, W. Kun, R. Yuan, C. Xiaocen, M. Limei, and Z. Yong, "Optimization design of launch locking protective device (LLPD) based on carbon fiber bracket for magnetically suspended flywheel (MSFW)," *Acta Astronautica*, vol. 154, pp. 9–17, Jan. 2019.

[11] X. Xu, J. Fang, and T. Wei, "Stability analysis and imbalance compensation for active magnetic bearing with gyroscopic effects," in *Proc. 8th IEEE Int. Symp. Instrum. Control Technol. (ISICT)*, London, U.K., Jul. 2012, pp. 295–300.

[12] R. Herzog, P. Buhler, C. Gahler, and R. Larsonneur, "Unbalance compensation using generalized notch filters in the multivariable feedback of magnetic bearings," *IEEE Trans. Control Syst. Technol.*, vol. 4, no. 5, pp. 580–586, Sep. 1996.

[13] C. Peng, J. Fang, and P. Cui, "Dynamics modeling and measurement of the microvibrations for a magnetically suspended flywheel," *IEEE Trans. Instrum. Meas.*, vol. 64, no. 12, pp. 3239–3252, Dec. 2015.

[14] H. A. DeSmidt, K. W. Wang, and E. C. Smith, "Multiharmonic adaptive vibration control of misaligned driveline via active magnetic bearings," *J. Dyn. Syst., Meas., Control*, vol. 130, no. 4, Jun. 2008, Art. no. 041006.

[15] J. I. Inayat-Hussain, "Nonlinear dynamics of a magnetically supported rigid rotor in auxiliary bearings," *Mechanism Mach. Theory*, vol. 45, no. 11, pp. 1651–1667, 2010.

[16] P. S. Keogh and M. O. T. Cole, "Rotor vibration with auxiliary bearing contact in magnetic bearing systems Part 1: Synchronous dynamics," *Proc. Inst. Mech. Eng., C, J. Mech. Eng. Sci.*, vol. 217, no. 4, pp. 1989–1996, Apr. 2003.

[17] C. Peng, J. Sun, C. Miao, and J. Fang, "A novel cross-feedback notch filter for synchronous vibration suppression of an MSFW with significant gyroscopic effects," *IEEE Trans. Ind. Electron.*, vol. 64, no. 9, pp. 7181–7190, Sep. 2017.
[18] P. Cui, S. Li, Q. Wang, Q. Gao, J. Cui, and H. Zhang, "Harmonic current suppression of an AMB rotor system at variable rotation speed based on multiple phase-shift notch filters," *IEEE Trans. Ind. Electron.*, vol. 63, no. 11, pp. 6962–6969, Nov. 2016.
[19] X. Xu, S. Chen, and Y. Zhang, "Automatic balancing of AMB systems using plural notch filter and adaptive synchronous compensation," *J. Sound Vib.*, vol. 374, pp. 29–42, Jul. 2016.
[20] T. Mizuno, T. Higuchi, "Design of magnetic bearing controllers based on disturbance estimation," in *Proc. of the 2nd Int. Symp.*, Tokyo, Japan, Jul. 1990, pp. 281–288.
[21] X. Sun, B. Su, L. Chen, Z. Yang, X. Xu, and Z. Shi, "Precise control of a four degree-of-freedom permanent magnet biased active magnetic bearing system in a magnetically suspended direct-driven spindle using neural network inverse scheme," *Mech. Syst. Signal Process.*, vol. 88, pp. 36–48, May 2017.
[22] J. Shi, R. Zmood, and L. J. Qin, "The direct method for adaptive feed-forward vibration control of magnetic bearing systems," in *Proc. 7th Int. Conf. Control, Automat., Robot. Vis.*, Dec. 2002, pp. 675–680.
[23] C. Bi, D. Wu, Q. Jiang, and Z. Liu, "Automatic learning control for unbalance compensation in active magnetic bearings," *IEEE Trans. Magn.*, vol. 41, no. 7, pp. 2270–2280, Jul. 2005.
[24] B. Liu, J. Fang, G. Liu, and Y. Fan, "Unbalance vibration control and experiment research of magnetically suspended flywheels," *J. Mech. Eng.*, vol. 46, no. 12, pp. 188–194, Jan. 2010.
[25] T. Wei and M. Xiang, "Autobalancing for magnetically suspended high-speed rotors based on lead feedforward compensation for displacement stiffness force," *J. Mech. Eng.*, vol. 48, no. 16, pp. 184–192, Aug. 2012.
[26] S. Zheng, B. Han, R. Feng, and Y. Jiang, "Vibration suppression control for AMB-supported motor driveline system using synchronous rotating frame transformation," *IEEE Trans. Ind. Electron.*, vol. 62, no. 9, pp. 5700–5708, Sep. 2015.
[27] S. Kallio, M. Andriollo, A. Tortella, and J. Karttunen, "Decoupled d-q model of double-star interior-permanent-magnet synchronous machines," *IEEE Trans. Ind. Electron.*, vol. 60, no. 6, pp. 2486–2494, Jun. 2013.
[28] A. Pigazo, V. M. Moreno, and E. J. Estébanez, "A recursive park transformation to improve the performance of synchronous reference frame controllers in shunt active power filters," *IEEE Trans. Power Electron.*, vol. 24, no. 9, pp. 2065–2075, Sep. 2009.

CONG PENG received the B.S. degree from Southeast University, Nanjing, China, in 2010, and the Ph.D. degree in instrument science and technology from Beihang University, Beijing, China, in 2016.

She is currently a Research Member with the College of Automation Engineering, Nanjing University of Aeronautics and Astronautics. Her research interests include robust control of the magnetic bearing systems and the active vibration control of the magnetically suspended actuators.

QIAN ZHOU received the B.S. degree from the School of Automation, Nanjing Institute of Technology, Nanjing, China, in 2017.

He is currently pursuing the M.S. degree with the College of Automation Engineering, Nanjing University of Aeronautics and Astronautics, Nanjing. His research interest includes the active vibration control of the magnetically suspended actuators.